

# Dual-pulse Laser Induced Breakdown Spectroscopy for analysis of gaseous and aerosol systems: Plasma-analyte interactions

B.C. Windom, P.K. Diwakar, D.W. Hahn \*

*Department of Mechanical and Aerospace Engineering, University of Florida, Gainesville, FL 32611-6300, United States*

Received 5 April 2006; accepted 5 June 2006

Available online 2 August 2006

## Abstract

Dual-pulse LIBS has been previously investigated to a large extent on solid and liquid phase analytes, where it has been demonstrated to significantly enhance atomic emission signal intensity, and more importantly, to enhance the analyte peak-to-base and signal-to-noise ratios. This study focuses on the effects of an orthogonal dual-pulse laser configuration on the atomic emission response for both purely gaseous and calcium-based aerosol samples. The gaseous sample consisted of purified (i.e. aerosol free) air, from which nitrogen and oxygen spectral emission lines were analyzed. Measurements for the gaseous system resulted in no notable improvements with the dual-pulse configuration as compared to the single-pulse LIBS. Experiments were also conducted in purified air seeded with calcium-rich particles, which revealed a marked improvement in calcium atomic emission peak-to-base (~ 2-fold increase) and signal-to-noise ratios (~ 4-fold increase) with the dual-pulse configuration. In addition to increased analyte response, dual-pulse LIBS yielded an enhanced single-particle sampling rate when compared to conventional LIBS. Transmission measurements with respect to the plasma-creating laser pulse were recorded for both single and dual-pulse methods over a range of temporal delays. In consideration of the spectroscopic and transmission data, the plasma-analyte interactions realized with a dual-pulse methodology are explained in terms of the interaction with the initially expanding plasma shock wave, which differs between gaseous and particulate phase analytes, as reported in a recent study [V. Hohreiter, D.W. Hahn, Calibration effects for laser-induced breakdown spectroscopy of gaseous sample streams: analyte response of gas-phase species versus solid-phase species, *Anal. Chem.* 77 (2005) 1118–1124].

© 2006 Elsevier B.V. All rights reserved.

*Keywords:* Laser-induced breakdown spectroscopy; LIBS; Aerosol; Dual-pulse

## 1. Introduction

Due to the relative experimental simplicity and immediate analyte response, laser-induced breakdown spectroscopy (LIBS) has gained popularity as a technique among researchers interested in real time or *in situ* material detection and analysis for a wide range of sample forms including solids, liquids, gases, and aerosol systems. A recent review paper traces the origins of LIBS and its emergence as an accepted analytical technique [2]. For many applications of LIBS, it is important to enhance the detection of atomic spectral lines by increasing the analyte signal while minimizing the background continuous emission (i.e. by improving the sensitivity and detection limits). Toward this end, there have been many research efforts focused on methods to further elucidate and improve the LIBS analyte response.

The dual-pulse LIBS configuration has been one such method. While the first use of an additional laser pulse to reheat the plasma dates back to the early 1990s [3], in recent years significant efforts among many research groups have focused on enhancing laser–solid interactions, atomic emission intensity, and detection limits with dual-pulse techniques [4–15]. Often used, including in the current study, is an orthogonal dual-pulse LIBS methodology. This configuration involves two excitation lasers aligned perpendicular to each other, which enables the formation of temporally separated plasmas (separations ranging from nanoseconds to microseconds apart) on or near the sample of interest. To date, contemporary dual-pulse LIBS studies have all focused on solid or liquid phase analytes, where reported spectral enhancements have been as much as 40 times greater as compared to single LIBS configurations [4,9,10,12,14]. Recent studies have examined the mechanisms for this dual-pulse enhancement, focusing on the laser–solid coupling [14,15], as well as the hydrodynamics of the overlapping laser pulses, shock

\* Corresponding author.

E-mail address: [dwhahn@ufl.edu](mailto:dwhahn@ufl.edu) (D.W. Hahn).

waves, and subsequent density effects [11]. The exact mechanisms of signal enhancement with dual-pulse LIBS are complex due to the combinations of laser ablation, analyte dissociation, and plasma excitation of atomic species. Previous studies have shown that enhancements in atomic emission intensity, peak-to-base, and signal-to-noise measurements with a dual-pulse system are not simply the result of added energy from the pre-ablation laser-induced plasma. In fact, dual-pulse signal enhancements are coupled to other physical phenomena such as enhanced ablation, shock-induced plasma rarefaction (i.e. reduced density), or thermal lensing from the pre-ablation plasma [9,10,14,15]. While much has been learned from these studies of solids and liquids, the extension of dual-pulse LIBS to gas-phase and aerosol systems brings along a new set of dynamics which have not been explored to date.

The present study is concerned with quantifying signal enhancement of LIBS by implementing an orthogonal dual-pulse configuration for purely gaseous and aerosol systems. In addition to documenting the overall behavior with regard to analyte emission response, efforts are made to elucidate the physical mechanisms for dual-pulse behavior in consideration of recent work on the differences in analyte response between gas-phase and aerosol-phase analytes [1].

## 2. Experimental methods

### 2.1. Laser configuration

Two Q-switched Nd:YAG lasers operating at their fundamental wavelength of 1064 nm and at a repetition rate of 5 Hz were used for all experiments. Both beams were expanded and collimated to increase the beam diameter, thereby allowing for a tighter focus and more consistent plasma location. A schematic of the optical configuration is shown in Fig. 1. The first laser (Continuum Precision II 8000), which will be referred to as *Laser 1*, used a laser beam energy of 100 mJ/pulse, and was focused to the center of the sample chamber (a six-way vacuum cross) using a 100-mm focal length lens. The pulse-to-pulse stability was directly measured (Ophir Nova II), which yielded a relative standard deviation (RSD) of 0.42%, with a maximum pulse deviation of

1.4%. The pulse energy was sufficient to create a laser-induced plasma with *Laser 1* operating alone in either a purely gas-phase or aerosol laden sample stream. The second laser (Big Sky CFR 400), which will be referred to as *Laser 2*, operated at a laser pulse energy of 290 mJ/pulse, and was focused with a 75-mm focal length lens, also creating a laser-induced breakdown in the center of the six-way cross. The pulse-to-pulse stability was (RSD) of 0.45%, with a maximum pulse deviation of 1.5%.

The two laser beams were carefully aligned such that the two plasmas were formed at the identical spatial location (see below for alignment details). No quantitative plasma volume measurements were recorded. However, the *Laser 2* plasma was previously characterized in detail; hence a characteristic plasma diameter is reported as 1.5 mm [16]. Furthermore, the *Laser 2* plasma was noticeably larger than the *Laser 1* plasma, presumably due to the greater laser pulse energy.

The flashlamp sync of *Laser 1* was used to trigger a digital delay generator, which was then subsequently used to trigger the flashlamp and Q-switch of *Laser 2*. Adjustment of the delay generator allowed for the two laser pulses to fire simultaneously, or at variable pulse-to-pulse delays ranging up to 1 ms, the largest investigated. For all experiments, the delay was adjusted such that *Laser 1* was fired first, followed by *Laser 2* at the specified delay. The relative flashlamp to Q-switch timing was maintained constant for both lasers for all experiments, thereby ensuring constant laser pulse energy and laser beam characteristics. It is noted that a delay time of zero corresponds to both *Laser 1* and *Laser 2* pulses firing simultaneously. A fast response (200-ps rise time) detector and digital oscilloscope (2.5 Gsample/s) were used to continuously measure and monitor the temporal delay between the two laser pulses for all experiments. As implemented, the jitter between *Laser 1* and *Laser 2* was typically less than 5 ns.

### 2.2. Analyte generation

All analyte samples flowed through a standard six-way vacuum cross at atmospheric pressure, which functioned as the LIBS sample chamber as previously described [17,18]. The purely gaseous sample stream consisted of 40 lpm of purified air, which was passed through an activated alumina dryer, a course

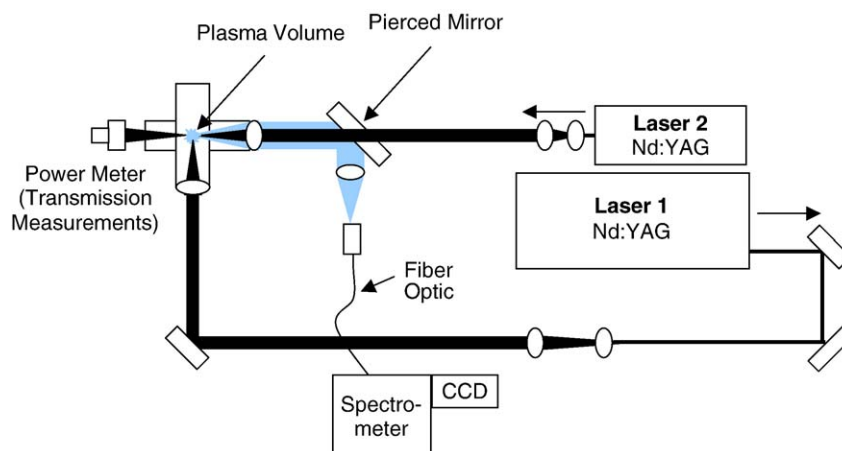


Fig. 1. Experimental apparatus for single and dual-pulse LIBS configurations.

particle filter, an additional desiccant dryer, and finally a HEPA filter cartridge prior to entering the sample chamber. All flow rates were controlled with digital mass flow controllers.

For the aerosol measurements, two types of calcium-containing particles were used, with the purpose of studying any potential size effects. The majority of aerosol measurements were made by nebulizing a solution of 50-micrograms Ca/ml at a rate of about 0.1 ml/min. The nebulizer output was introduced in a gaseous co-flow stream of 40 lpm of purified air. The calcium solutions were prepared by diluting ICP-grade analytical standards of 10,000  $\mu\text{g Ca/ml}$  (SPEX CertiPrep). Accounting for the additional 5 lpm used to drive the nebulizer, this configuration resulted in a calcium-rich aerosol flow of approximately  $100 \mu\text{g Ca/m}^3$  through the LIBS sample chamber. Based on previous TEM measurements using the current configuration [18], the average aerosol particle size following droplet desolvation (i.e. solid analyte phase) is expected to be less than 100 nm, while agglomerate formation is considered insignificant. The corresponding particle number density is on the order of  $10^5 \text{ cm}^{-3}$  in the LIBS sample chamber, which yields an average number of analyte particles per plasma volume on the order of 100. Overall, the system provides a highly dispersed, submicron-sized calcium-rich aerosol stream for LIBS analysis. This analyte source will be referred to as the fine calcium aerosol experiments.

In addition, some experiments were performed by nebulizing a suspension of nominally 2- $\mu\text{m}$  sized ( $\pm 0.5 \mu\text{m}$ ) borosilicate glass microspheres (Duke Scientific, #9002) in ultrapurified water. Based on previous analysis, the calcium concentration within the glass microspheres was determined to be about 2% (by mass), which yields a strong calcium atomic emission signal [19]. The particle concentration in suspension was adjusted so that the resulting borosilicate particle number density produced in the LIBS sample chamber was on the order of  $10^2 \text{ cm}^{-3}$ . These experimental conditions will be referred to as the borosilicate microsphere experiments.

### 2.3. Spectral measurements

Spectral emission from the laser-induced plasma was collected via backscatter by a pierced mirror and focused onto a fiber optic bundle, as shown in Fig. 1, and subsequently coupled to the spectrometer. The light was then dispersed by the 0.275-m spectrometer (Acton SpectraPro-275) and finally recorded by a  $256 \times 1024$  element intensified CCD array. The spectrometer used a 2400-groove/mm grating, which provided an approximately 30-nm wavelength range with 0.12-nm spectral resolution.

Both laser-induced plasmas were first visually aligned to the same spot, noting that the Laser 2 plasma emission was previously aligned to the fiber optic such that both atomic and continuum plasma emission were optimized. Once the Laser 1 plasma was visually centered on the Laser 2 plasma, the final alignment of Laser 1 was performed to maximize plasma emission (atomic and continuum emission) coupling to the fiber optic, thereby ensuring alignment of both laser-induced plasmas to the same spatial location.

For all single-pulse and dual-pulse experiments, the external Q-switch sync from Laser 2 was used to trigger the ICCD con-

troller. Hence for a given set of experiments, the ICCD was fixed relative to the temporal position of Laser 2. The ICCD gate (i.e. detector delay and width) was then synchronized to Laser 2, which allowed for optimization of the specific analyte atomic emission signals. For the purely gas-phase experiments (i.e. nitrogen and oxygen atomic emission analysis), an ICCD gate delay and gate width of 5  $\mu\text{s}$  were used, therefore spectral integration was initiated 5  $\mu\text{s}$  following Laser 2. For the aerosol experiments (i.e. calcium atomic emission analysis), both the detector delay and the gate width were increased to 30  $\mu\text{s}$ .

Spectral data was acquired using an ensemble average of 1000 laser shots. The process was repeated a total of three times for each different analyte, and for each adjusted dual-pulse delay. In addition to dual-pulse measurements, single-pulse data were recorded for both Laser 1 alone and Laser 2 alone for all different analytes. Finally, single-particle analysis was used for the 2- $\mu\text{m}$  sized borosilicate glass particles, as reported in previous studies [17,19]. These single-shot experiments were performed using 500 shot sequences, repeated three times for each experimental condition.

### 2.4. Transmission measurements

For the transmission experiments, laser pulse energy measurements were made for Laser 2 at a spatial location directly in front of the sample chamber (i.e. incident energy) and at a location directly exiting the sample chamber (i.e. transmitted energy). This was achieved by placing the laser energy meter (Ophir Nova II) in front of the sixway cross to measure the incident beam energy, and immediately after the chamber to measure the transmitted laser beam energy, with the latter configuration shown in Fig. 1. The average transmitted energy (i.e. Laser 2 transmission) was then calculated from the direct ratio of these two measurements.

The transmission measurements were recorded for both single-pulse (Laser 2 only) and dual-pulse (Laser 2 following Laser 1) configurations, for both the gaseous and aerosol systems, including a full range of dual-pulse, laser-laser delay times. An ensemble-average of 500 laser shots was recorded for both the incident and transmitted pulse energies, which were repeated a minimum of three times each. In addition to the mean energy values, full statistical parameters were recorded, which included the minimum, maximum, and standard deviations of the shot-to-shot pulse energies.

## 3. Experimental results and discussion

### 3.1. Transmission experiments

Fig. 2 presents the transmission of Laser 2 as a function of delay time between Laser 1 and Laser 2 for both the pure air stream and the fine calcium aerosol experiments. As a reference, the dashed line in Fig. 2 represents the average transmission of 43.8% for the single-pulse configuration (i.e. Laser 2 only), which is the average of the purified air (44.5% with 2.7% RSD) and the fine calcium particle (43.1% with 0.8% RSD) transmission values. The overall behavior of the transmission data as observed in Fig. 2 is rather complex, and is considered for

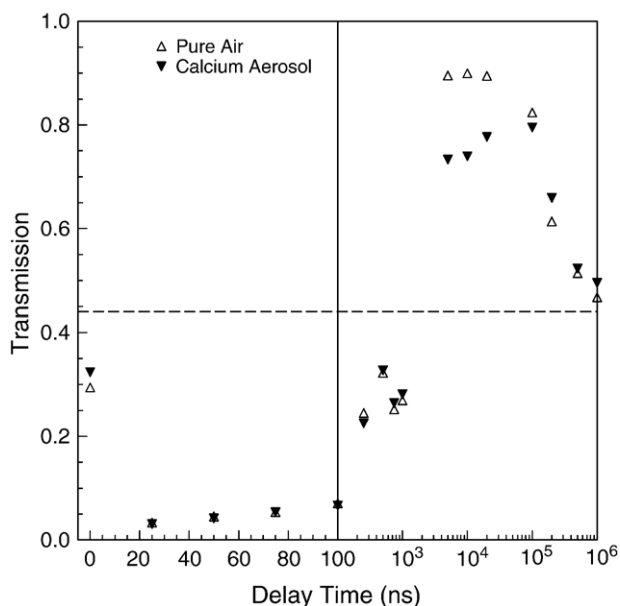


Fig. 2. Laser 2 transmission as a function of dual-pulse laser delay times for the pure air and fine calcium aerosol sample streams. The horizontal line represents the transmission of Laser 2 alone (i.e. single-pulse LIBS). Note the plot is linear for delay times less than 100 ns.

discussion purposes in terms of four distinct temporal regions. The average RSD values for the dual-pulse transmission measurements were 4.4% for the pure air stream and 3.3% for the fine calcium particles, as averaged over all temporal delays. The corresponding error bars were comparable to the symbol size for most values, hence error bars were omitted in Fig. 2 to avoid clutter, given the partial overlap of many symbols.

The first temporal region to be considered will correspond to dual-pulse delays less than 100 ns. During this temporal range, there was little transmission of Laser 2 through the plasma formed by Laser 1, as explained below. The minimum recorded transmission was 3.4% (1.3% RSD) and 3.1% (8.2% RSD), which both occurred at a delay of 25 ns, for the gas-phase and fine calcium aerosol phase, respectively. At these delays, the plasma formed by Laser 1 is essentially opaque to the incident Laser 2 pulse, which follows a previously reported trend for the temporal characteristics of laser-induced plasmas [20]. During this temporal region, the high plasma temperatures and free electron densities ( $\sim 10^{18} \text{ cm}^{-3}$ ) of the first plasma result in an optically dense plasma for the Laser 2 incident radiation. The resulting highly energetic plasma state is essentially independent of the presence of the calcium aerosol, therefore no difference is observed between the two experimental conditions. This result is consistent with previous measurements, in which identical plasma temperatures and free electron densities were recorded for gas-phase and particle-seeded flows under conditions similar to the present study [1], and no effect of aerosol presence on the temporal location of plasma initiation was recorded [21]. Finally, it is noted that qualitative observations of the plasma revealed no differences between the pure air and the aerosol seeded conditions, with regard to plasma size and spatial stability.

The second temporal region of interest in Fig. 2 is considered to range from a delay of 100 ns to about 1  $\mu\text{s}$ . During this region, the highly absorptive nature of the first plasma decreases as the free electron density and temperature rapidly decrease. Once again, this is consistent with previous measurements, where an essentially identical laser-induced plasma was found to be nearly transparent to a low-energy probe beam by about 500 ns following plasma initiation [20]. Within this temporal period, the plasma frequency ( $\nu_p$ ) has fallen to the order of  $10^{12}$  Hz. The plasma frequency is the reciprocal of the Debye length, and represents the resonance frequency of the free electron oscillations about their equilibrium positions. Such a relatively low plasma frequency is consistent with the concomitant drop in absorptivity, as expected for the condition of  $\nu_p \ll \nu_{\text{incident}}$ . Overall, as the delay between Laser 1 and Laser 2 nears about 1  $\mu\text{s}$ , the effect of the Laser 1 plasma is not very significant regarding the coupling of Laser 2 energy into the existing Laser 1 plasma, as the overall transmission of Laser 2 is near its single-pulse value. In other words, with the dual-pulse configuration, Laser 2 initiates a breakdown process comparable to what would occur in the presence of Laser 2 alone, resulting in a similar coupling of the incident energy into the resulting plasma.

The third temporal region corresponds to delays ranging from 1  $\mu\text{s}$  to about 100  $\mu\text{s}$ , and is defined by a relatively high transmission of the Laser 2 pulse. Specifically, the transmission of Laser 2 has a maximum value of 90.0% (0.82% RSD) and 79.5% (1.1% RSD) for the pure air and fine calcium aerosol systems, respectively, over this temporal region. Unlike in the earlier temporal regions, an effect of the fine calcium aerosol is now observed, as the transmission is slightly reduced in the presence of aerosol in comparison to the pure gaseous system. This reduction is indicative of some laser-particle interactions during the breakdown event, as discussed in more detail below.

Finally, the fourth temporal region corresponds to laser-laser delays from 100  $\mu\text{s}$  up to 1 ms. At the latter value, the transmission of the Laser 2 beam is observed to approach the average single-pulse (i.e. Laser 2 only) value. Clearly at such large delays, the Laser 1 plasma has sufficiently decayed in both temperature and free electron density such that its effects on the subsequent laser pulse (i.e. Laser 2) are negligible.

The transmission behavior of the first two regions is not unexpected, given the earlier studies on temporal plasma characteristics; hence a strong plasma-laser interaction during this period drives the dual-laser coupling and is virtually independent of the presence of particulates. Furthermore, the behavior of the last region is expected as well, given that at significantly long laser-laser delays, the two lasers pulses must approach independence with regard to interaction. Clearly  $\sim 1$  ms is nearing this asymptotic limit for pulse-to-pulse independence. Given these comments, a key region of interest with regard to the physics of dual-pulse LIBS for gaseous and aerosol systems is the third region, namely between about 1 to 100  $\mu\text{s}$  of laser-laser delay. It is well known that the laser-induced plasma is characterized by a rapid plasma expansion and a concomitant shock wave. Notwithstanding the increased pressure behind the shock front, the significant plasma temperature results in a reduced density (i.e. mass/

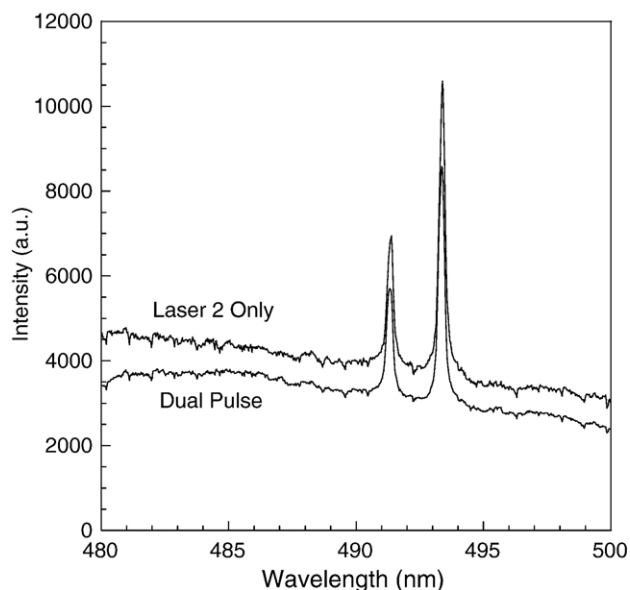


Fig. 3. Spectra showing the two nitrogen atomic emission lines at 491.4 nm and 493.5 nm. The spectra correspond to dual-pulse LIBS with 500-ns delay (lower spectrum) and single-pulse (Laser 2 only) LIBS (upper spectrum). Both spectra have the same scale.

volume) within the resulting plasma. This rarefaction is important with regard to the coupling of Laser 2 into the existing Laser 1 plasma, as related to the breakdown threshold. At ambient temperature, the laser-induced breakdown threshold is known to vary inversely as pressure, ideally as  $p^{-1/2}$ , noting that both multiphoton and cascade ionization processes are important in plasma formation and growth. Therefore, the ionized plasma from Laser 1, albeit at reduced density, presents a more complex problem for treatment of the Laser 2 interaction than would be predicted from treatment of pressure/density effects alone. However, the significant decrease in Laser 2 energy coupling into the plasma (i.e. increased transmission) is interpreted in terms of an increased breakdown threshold. This increased threshold effectively delays the temporal “breakdown” point of the Laser 2 pulse to later in the pulse waveform, thereby resulting in less coupling of Laser 2 pulse energy. It is well known that the presence of aerosol particles can considerably lower the breakdown threshold. Therefore, the slight reduction in transmission between 5 and 20  $\mu\text{s}$  delay from the pure air stream ( $\tau=89.7\%$  with 0.7% RSD) as compared to the fine aerosol stream ( $\tau=75.0\%$  with 1.5% RSD) is consistent with the addition of the calcium-rich particulates and a concomitant reduction in breakdown threshold.

### 3.2. Spectral analysis of gaseous analytes

Neutral atomic nitrogen (N I) lines at 491.4 nm and 493.5 nm ( $86,137\text{--}106,178\text{ cm}^{-1}$  and  $86,221\text{--}106,478\text{ cm}^{-1}$ , respectively), and the oxygen triplet centered at 394.7 nm ( $73,768\text{--}99,094\text{ cm}^{-1}$ ) were used for the spectral analysis of the purified air sample stream. As an example, nitrogen spectra for the single-pulse (Laser 2 only) and the dual-pulse (500 ns delay) configurations are presented in Fig. 3. Recalling that the ICCD is also synchronized to Laser 2, it is observed that the overall

signal intensity is somewhat reduced by the dual-pulse scheme for this temporal regime. However, at significantly short laser–laser delay times ( $\sim 0$  to 100 ns), the dual-pulse configuration produced a slightly greater emission intensity than Laser 2 alone, which is consistent with the enhanced coupling efficiency of Laser 2 as observed in the transmission experiments.

To quantify the emission signals, both the peak-to-base and signal-to-noise ratios were calculated using the 493.5-nm N I spectral line for both the dual-pulse and the single-pulse configurations. The peak-to-base is perhaps the most widely used LIBS signal metric, as it provides a normalization of the atomic emission line with the plasma continuum emission, allowing for a more precise emission signal as noted previously [10,22]. As an analytical figure of merit, the signal-to-noise ratio is the more relevant metric. The signal-to-noise ratios (SNR) were calculated from the integrated peak intensities and the calculated root-mean-square noise from the adjacent continuum region. Figs. 4 and 5 present the peak-to-base ratio ( $P/B$ ) and signal-to-noise ratio as a function of dual-pulse delay for the 493.5-nm nitrogen line. Before discussing the figures, it is important to note that Laser 1 alone produces a significant laser-induced plasma; hence analyte emission is observed over a range of detector gate delays stemming from this emission source only. Therefore, as the laser–laser delay is being adjusted for dual-pulse experiments, the effective detector gate delay with respect to Laser 1 is also being varied, noting that the detector gate is fixed with respect to Laser 2. It is therefore important to consider the analyte signals stemming from Laser 1 alone (i.e. Laser 2 blocked), which are therefore included in Figs. 4 and 5.

Fig. 4 shows the dual-pulse results as compared to the single-pulse LIBS configuration (i.e. Laser 2 only), which is indicated with the dashed horizontal line. For the range of delays from 0

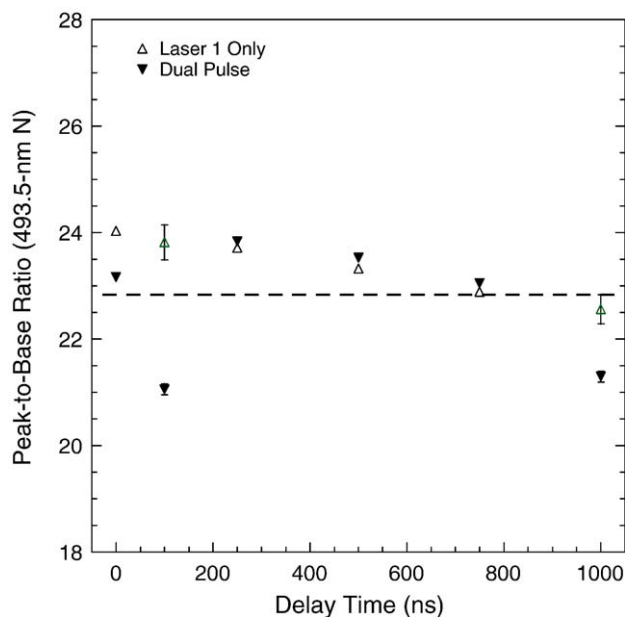


Fig. 4. 493.5-nm nitrogen emission line peak-to-base ratio measurements for the pure air sample as a function of dual-pulse laser delay times. The  $P/B$  ratios are also shown corresponding to the Laser 1 plasma only (i.e. Laser 2 beam blocked). The dashed horizontal line represents the average  $P/B$  ratio for Laser 2 only.

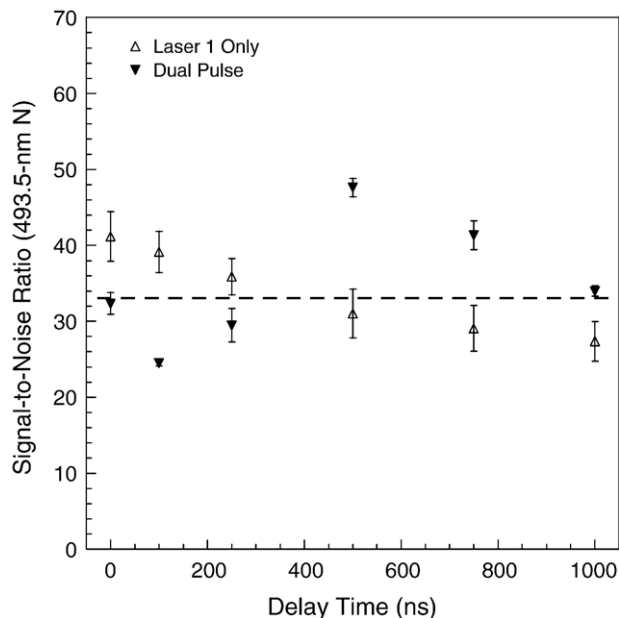


Fig. 5. 493.5-nm nitrogen emission line signal-to-noise ratio measurements for the pure air sample as a function of dual-pulse laser delay times. The SNR is also shown corresponding to the Laser 1 plasma only (i.e. Laser 2 beam blocked). The dashed horizontal line represents the average SNR ratio for Laser 2 only.

to 1000 ns, the  $P/B$  ratios are observed to depart little from the single-pulse average of 22.8 (0.21% RSD). The maximum dual-pulse value occurs at 250 ns delay, and corresponds to a  $P/B$  ratio of 23.8 (0.41% RSD), or a 4% increase with the dual-pulse configuration. While statistically significant, a 4% signal enhancement would not justify the increased experimental complexity of the dual-pulse scheme. By 1  $\mu$ s delay time, the dual-pulse  $P/B$  ratio has decreased to 21.3 (0.47% RSD), or a reduction of 6.8% with regard to single-pulse LIBS. Data were collected for larger laser–laser delay times, but this trend of decreasing response continued, with a dual-pulse  $P/B$  ratio of only 9.3 (0.50% RSD) recorded at 5  $\mu$ s delay. This corresponds to a 60% decrease in analyte signal with the dual-pulse scheme at this larger delay, as a result of the diminished Laser 2 coupling consistent with Fig. 2.

The SNR values, as shown in Fig. 5, display a similar trend to the  $P/B$  ratios, although the maximum enhancement for the dual-pulse configuration is shifted from 250 ns delay to a delay of 500 ns. Specifically, the SNR is increased from a single-pulse value of 33.0 (0.47% RSD) to a dual-pulse value of 47.6 (2.4% RSD) at 500 ns, which corresponds to a 44% improvement. Once again, by a 5  $\mu$ s laser–laser delay, the dual-pulse SNR was decreased by 86%, to a value of only 4.6 (0.10% RSD).

The oxygen atomic emission lines revealed similar, although not as positive, trends as the nitrogen data. The  $P/B$  ratios were calculated using the 394.7-nm O I triplet. For a laser–laser delay of 250 ns, the  $P/B$  ratio was decreased from a single-pulse value of 18.1 (0.79% RSD) to a dual-pulse value of 17.0 (0.40% RSD), or a decrease of 6.5%. By 5  $\mu$ s, the dual-pulse  $P/B$  ratio was reduced to 4.2 (8.1% RSD), corresponding to a reduction of 76.9%.

The above results appear at first glance to contrast with much of the current literature on dual-pulse LIBS, which tends to show significant signal enhancements with dual-pulse schemes. How-

ever, the mechanisms and physics of purely gas-phase LIBS analysis are fundamentally different from the analysis of bulk solids or liquids. With the latter, the reduced density behind the shock wave of the first plasma *enhances* the second laser's interaction with the solid sample, while simultaneously *reducing* the plasma coupling with the gaseous matrix; thereby increasing the analyte response of the solid. In contrast, the present results must be explained in the context of the transmission experiments, as well as in terms of recent experiments comparing the response of gas-phase and particulate phase analytes [1].

For the relatively short laser–laser delay times ( $\approx 1 \mu$ s), the Laser 2 pulse is efficiently coupled to the Laser 1 plasma, leading to a greater quantity of energy coupled into the resulting dual-pulse plasma. Increased total laser pulse energy into a laser-induced plasma event may or may not improve the analyte signal response, as explored in detail in an earlier study [22], depending on the overall plasma regime. In the current study, the additional energy with the dual-pulse configuration produced a marginal increase in nitrogen emission, and a marginal decrease in oxygen emission, during this delay period. This trend most likely reflects the slightly different upper energy states of the nitrogen and oxygen transitions, which are expected to correspond to slightly different optimal temporal windows, as based on plasma temperature [23]. By coupling more energy into the resulting dual-pulse plasma, the temporal temperature profile of the plasma is altered, thereby altering the peak-to-continuum emission characteristics at the fixed detector gate. This behavior is further reflected by comparing the Laser 1 only data to the Laser 2 only data at zero delay time, which has the effect of changing the laser pulse energy from 100 mJ to 290 mJ with a fixed detector gate. The nitrogen  $P/B$  ratio is observed to decrease by 5% with increased pulse energy, while the oxygen  $P/B$  ratio is observed to increase by 3%. Clearly the temporal location of optimal  $P/B$  response is different for the selected nitrogen and oxygen emission lines.

Notwithstanding the above comments, for the longer laser–laser delay times (beyond 1  $\mu$ s), a very different dynamic is observed for both gaseous analyte species. Specifically, for this increased delay regime, the dual-pulse configuration yielded a significant decrease in analyte response, which again is explained in the context of Fig. 2, and the generally lessened LIBS analyte response with gas-phase species as recently reported [1]. In their study, Hohreiter and Hahn proposed that the expanding shockwave of the laser-induced plasma would preferentially expel (i.e. push) molecules from within the plasma core, producing a decreased concentration of analyte for gas-phase species. In addition to this depletion of analyte, the significantly reduced coupling of Laser 2 into the existing Laser 1 plasma (i.e. enhanced transmission per Fig. 2) effectively negates the dual-pulse advantage. This effect results in an analyte signal that, for the most part, corresponds to the Laser 1 plasma alone, as seen in the excellent agreement between the dual-pulse and Laser 1 only data in Figs. 4 and 5, as well as for the oxygen emission data. Stated another way, the dual-pulse advantage of de-coupling the gas-phase matrix from the bulk analyte phase, as realized with solid and liquid analysis, is not possible with a dual-pulse analysis of a purely gas-phase system, because the gas-phase matrix itself is the actual analyte of interest.

### 3.3. Spectral analysis of fine calcium-based aerosol analyte

In contrast to the above gas-phase analyte results, the analysis of the aerosol sample streams affords an opportunity to realize the benefits of dual-pulse LIBS by attempting to decouple the particulate-phase derived analyte from the gas-phase species. With the addition of aerosol particles into the sample stream, distinctly different results as compared to the gas-phase experiments were observed. For these experiments, the first ionized calcium (Ca II) atomic emission lines at 393.4 and 396.9 nm ( $0-25,414\text{ cm}^{-1}$  and  $0-25,192\text{ cm}^{-1}$ , respectively) were used for all spectral measurements due to their strong intensity. As an example, two recorded spectra are presented in Fig. 6, as acquired using the dual-pulse configuration with a laser–laser delay of 750 ns, and for comparison, using the single-pulse (Laser 2 only) configuration. Several features are noted. The relative intensity of the Ca II atomic emission peaks is significantly greater for the dual-pulse method as compared to the single-pulse method, namely 1980 counts vs. 1300 counts for the 393.4 nm peak, respectively. In addition, the region of the spectra to the left of 393.4-nm Ca II line corresponds to molecular emission from the  $N_2^+$  first negative system, including the lines at 391.4 and 388.4 nm. In contrast to the particle-derived calcium emission lines, these gas-phase derived molecular lines display an opposite trend, whereby the emission intensities are significantly reduced with the dual-pulse configuration. This latter trend is perfectly consistent with the above analysis of the gas-phase atomic nitrogen and oxygen emission data.

In a similar manner as for the gas-phase experiments (noting the longer detector gate and width of  $30\text{ }\mu\text{s}$ ), comparisons of Ca II atomic emission peak-to-base and signal-to-noise ratios were made for the single-pulse and dual-pulse configurations, with the results presented in Figs. 7 and 8, respectively. The dual-pulse

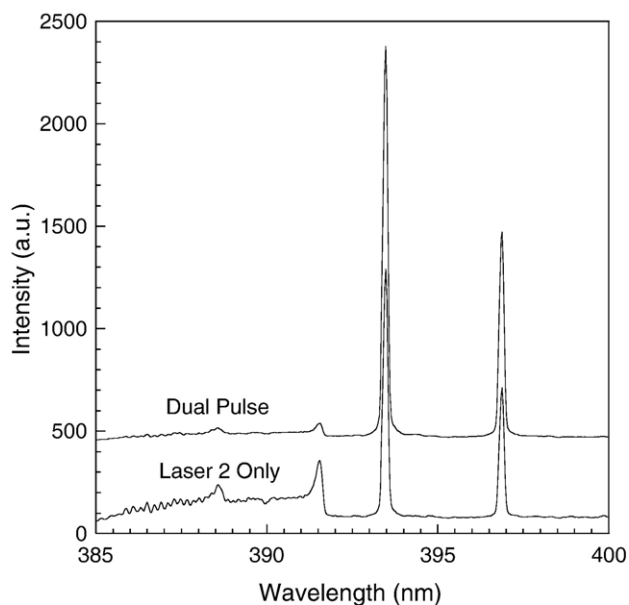


Fig. 6. Spectra showing the Ca II atomic emission lines at 393.4 and 396.9 nm for both the dual-pulse configuration with a 750-ns delay, and for Laser 2 only. Both spectra have the same intensity scale, and the dual-pulse spectrum has been shifted upward by 400 counts for clarity.

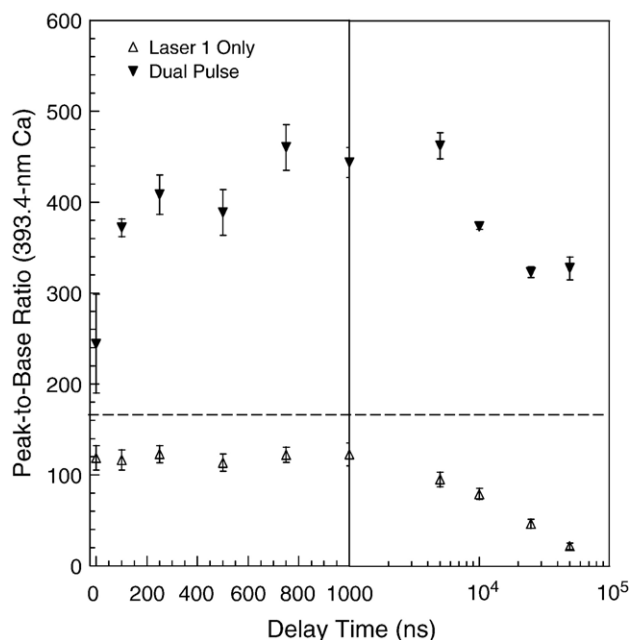


Fig. 7. 393.4-nm calcium II emission line peak-to-base ratio measurements for the fine calcium aerosol sample as a function of dual-pulse laser delay times. The  $P/B$  are also shown corresponding to the Laser 1 plasma only (i.e. Laser 2 beam blocked). The dashed horizontal line represents the average  $P/B$  ratio for Laser 2 only.

measurements for both the peak-to-base and signal-to-noise are significantly greater than those realized with the single-pulse scheme over a range of laser–laser delay times from about 100 ns to nearly  $100\text{ }\mu\text{s}$ . Specifically, the  $P/B$  ratio for the single-pulse experiments (Laser 2 only) was an average of 220 (7.0% RSD). With the dual-pulse configuration, the  $P/B$  was observed to increase to values of 460 (6.7% RSD) at 750 ns delay, and 463

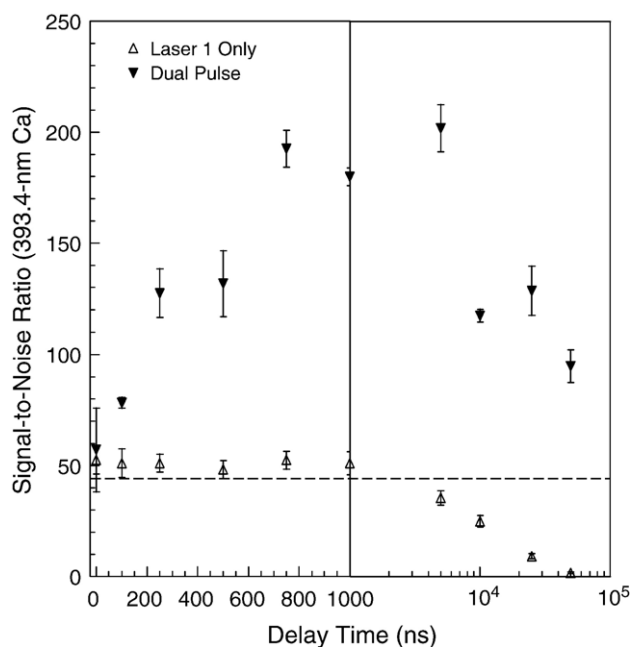


Fig. 8. 393.4-nm calcium II emission line signal-to-noise ratio measurements for the fine calcium aerosol sample as a function of dual-pulse laser delay times. The SNR are also shown corresponding to the Laser 1 plasma only (i.e. Laser 2 beam blocked). The dashed horizontal line represents the average SNR for Laser 2 only.

(4.6% RSD) at a delay of 5  $\mu\text{s}$ . Nearly identical trends were observed with the SNR data, as seen in Fig. 8. The average single-pulse (Laser 2 only) SNR value was 43.4 (7.1% RSD), which was increased to a maximum value of 202 (10.5% RSD) for a dual-pulse configuration with a laser–laser delay of 5  $\mu\text{s}$ . This corresponds to a greater than 4-fold increase in analyte sensitivity with the optimal dual-pulse scheme, which corresponds to a laser–laser delay in the range of about 0.8 to 5  $\mu\text{s}$ . It should also be noted that the Laser 1 (single laser only)  $P/B$  and SNR data are all markedly less than the dual-pulse results. The Laser 1 response corroborates the dual-pulse enhancement, and results from a steady decrease in calcium emission response with increasing laser-to-detector delay time, as effectively realized with the Laser 1 only experiments. Recall that with Laser 1 only, the detector gate is still being temporally delayed even though the Laser 2 beam is blocked. It has been well established that analyte species have an optimal temporal region, as related above, which is in agreement with this trend.

As discussed above with the purely gas-phase data, the aerosol-phase experiments should also be explained in the context of the transmission experiments and the recent gas-phase vs. particulate-phase analyte response study [1]. Referring once again to this earlier study, the solid particulates (i.e. aerosol phase analyte) were hypothesized to resist being driven from the plasma center along with the gaseous molecules by the expanding shock wave. The resulting “slip factor” has the effect of preferentially enhancing the particulate-phase/gas-phase analyte ratio, thereby affording an opportunity to enhance the analyte response of the solid phase with an optimally-timed second laser pulse. In other words, the gas-phase species within the plasma effectively contribute to the plasma continuum emission, hence to spectral noise with regard to the targeted particulate-derived analyte emission. In keeping with the Fig. 2 transmission data, the temporal region between about 1 and 10  $\mu\text{s}$  is consistent with a proposed mechanism in which the particulate-phase is preferentially enriched by the loss of gas-phase species, and is then additionally excited (i.e. strong coupling) by the second laser pulse (Laser 2). At relatively shorter delay times (<500 ns), the dual-pulse enhancement is not as great because the rarefaction has not yet developed, although plasma-laser coupling is still strong. At relatively longer delay times (>10–20  $\mu\text{s}$ ), the first plasma has undergone substantial decay, thereby reducing the coupling of Laser 2, and the system is once again approaching conditions corresponding to a single-pulse environment.

### 3.4. Spectral analysis of borosilicate glass microspheres

To further examine the observed phenomena of dual-pulse enhancement with aerosol analysis, in the context of the mechanisms offered above, additional experiments were performed using significantly larger aerosol particles, namely the 2- $\mu\text{m}$  borosilicate microspheres. This was done in an effort to determine if the plasma-particle interactions with the dual-pulse configuration were further enhanced with increasing particle size. Based on recent work with the identical particles, the overall time scale for particle dissociation within the laser-induced plasma was estimated to be on the order of 15  $\mu\text{s}$  [22], hence particulates are expected to be present during the current

tly determined optimal dual-pulse laser–laser delays of between about 1 and 10  $\mu\text{s}$ . For these experiments, suspensions of the borosilicate glass were nebulized as described above, and single-shot spectra were analyzed for the presence of calcium atomic emission using the same 393.4-nm Ca II atomic emission line. Measurements were made using a single-pulse configuration (Laser 2 only) and a dual-pulse configuration with a laser–laser delay of 250 ns. While this delay was not the optimal value per the SNR experiments, the single-shot detection criteria makes use of the  $P/B$  ratio [24]; hence the 250 ns was close to the optimal value per Fig. 7, and had the added advantage of slightly larger absolute signal counts to work with. Because the particle hit rate was adjusted (i.e. aerosol number density reduced) to be less than 100% to minimize multiple particle sampling with a single shot, any ensemble-averaging would reduce the effect of dual-pulse enhancement on calcium emission by averaging the calcium-containing spectra (i.e. particle hits) with non-calcium containing spectra (i.e. particle free spectra). Normally, this might be addressed by using a conditional processing routine to separate out the spectra corresponding to particle hits, and to then analyze only such spectra [25]. However, the easy solution of identifying and ensemble-averaging the spectra of calcium-based particle hits brings an additional problem. By enhancing the sensitivity of calcium detection with the dual-pulse configuration, the particle hit rate is expected to increase. However, since particle hits corresponding to the strongest calcium-emission signals are most likely to be sampled with both single-pulse and dual-pulse configurations, the gains in sampling rate with dual-pulse LIBS are expected to be made for the particle hits corresponding to the *weakest* calcium emission signals. Therefore, comparing an ensemble-average of a larger number of spectra that contain a larger percentage of weaker emission signals, to an average containing a smaller number of spectra but with stronger emission signals is not a valid comparison. Because development of a detailed algorithm to attempt to sort and categorize spectra according to emission signal distributions was beyond the scope of the present study, the borosilicate particle data were only analyzed in terms of the particle sampling rate. A comparison of the single-pulse to dual-pulse hit rate showed an increase by a factor of 2.6 (250% increase) with the dual-pulse configuration. This was based on the raw numbers of hits recorded using a thresholding algorithm as previously described [24]. In addition, all recorded single-shot spectra were then post-processed using both calcium emission lines (393.4 and 396.9 nm) in an attempt to reject spectra corresponding to false particle hits, as previously described [17]. Following this analysis, the ratio of particle hit rates with dual-pulse LIBS as compared to the single-pulse (Laser 2 only) configuration was again equal to 2.6, in exact agreement with the previous result. Overall, the borosilicate glass particle experiments were consistent with the above fine-particulate experiments, verifying that the dual-pulse LIBS configuration does produce an enhanced analyte response for the micron-sized particles as well.

In summary, the use of dual-pulse LIBS for the analysis of gaseous and aerosol systems displays a complex behavior that is explained in terms of the plasma-laser coupling, and in regard to

recent experiments that explore the nature of gas-phase and particulate-phase analytes in a laser-induced plasma. Based on the current analysis, clearly the dual-pulse LIBS approach is applicable to aerosol systems, namely the analysis of particulate-phase analytes. Under such conditions, the realized 4-fold analyte signal enhancements show promise as a way to improve detection limits for real-time aerosol sensing applications, and might justify the added system complexity of dual-pulse configurations for critical sensing needs. The rather poor response of dual-pulse LIBS for analysis of strictly gas-phase species provides additional insight into the physics of the plasma-analyte interactions, and further supports the concept of preferential analyte depletion within the expanding plasma for pure gas-phase analysis. Overall, continued efforts to enhance the understanding of laser-induced plasma interactions with analyte species are important for improvement in analyte emission response, developments in plasma modeling, and for the overall advancement of LIBS as a robust analytical method.

### Acknowledgments

This work was supported in part by the National Science Foundation through grant CTS-0317410.

### References

- [1] V. Hohreiter, D.W. Hahn, Calibration effects for laser-induced breakdown spectroscopy of gaseous sample streams: analyte response of gas-phase species versus solid-phase species, *Anal. Chem.* 77 (2005) 1118–1124.
- [2] L.J. Radziemski, From laser to LIBS, the path of technology development, *Spectrochim. Acta Part B* 57 (2002) 1109–1113.
- [3] J. Uebbing, J. Brust, W. Sdorra, F. Leis, K. Niemax, Reheating of a laser-produced plasma by a second pulse laser, *Appl. Spectrosc.* 45 (9) (1991) 1419–1423.
- [4] R. Sattman, V. Sturm, R. Noll, Laser-induced breakdown spectroscopy of steel samples using multiple Q-switch Nd:YAG laser pulses, *J. Phys., D. Appl. Phys.* 28 (1995) 2181–2187.
- [5] S. Nakamura, Y. Ito, K. Sone, Determination of an iron suspension in water by laser-induced breakdown spectroscopy with two sequential laser pulses, *Anal. Chem.* 68 (1996) 2981–2986.
- [6] L. St-Onge, M. Sabsabi, P. Cielo, Analysis of solids using laser-induced plasma spectroscopy in double-pulse mode, *Spectrochim. Acta Part B* 53 (1998) 407–415.
- [7] D.N. Stratis, K.L. Eland, S.M. Angel, Dual-pulse LIBS using a pre-ablation spark for enhanced ablation emission, *Appl. Spectrosc.* 54 (9) (2000) 1270–1274.
- [8] D.N. Stratis, K.L. Eland, S.M. Angel, Effect of pulse delay time on a pre-ablation dual-pulse LIBS plasma, *Appl. Spectrosc.* 55 (2001) 1297–1303.
- [9] S.M. Angel, D.N. Stratis, K.L. Eland, T. Lai, M.A. Berg, D.M. Gold, LIBS using dual- and ultra-short laser pulses, *Fresenius' J. Anal. Chem.* 369 (2001) 320–327.
- [10] F. Coloa, V. Lazic, R. Fantoni, S. Pershin, A comparison of single and double pulse laser-induced breakdown spectroscopy of aluminum samples, *Spectrochim. Acta Part B* 57 (2002) 1167–1179.
- [11] M. Corsi, G. Cristoforetti, M. Giuffrida, M. Hildago, S. Legnaioli, V. Palleschi, A. Salvetti, E. Tognoni, C. Vallebona, Three-dimensional analysis of laser-induced plasmas in single and double pulse configuration, *Spectrochim. Acta Part B* 59 (2004) 723–735.
- [12] J. Scaffidi, W. Pearman, M. Lawrence, J. Chance Carter, B.W. Colston, S.M. Angel, Spatial and temporal dependence of interspark interactions in femtosecond–nanosecond dual-pulse laser-induced breakdown spectroscopy, *Appl. Opt.* 43 (27) (2004) 5243–5250.
- [13] C. Gautier, P. Fichet, D. Menut, J.-L. Lacour, D. L'Hermite, J. Dubessy, Quantification of the intensity enhancements for the double-pulse laser-induced breakdown spectroscopy in the orthogonal beam geometry, *Spectrochim. Acta Part B* 60 (2005) 265–276.
- [14] V. Hohreiter, D.W. Hahn, Dual-pulse laser-induced breakdown spectroscopy: time-resolved transmission and spectral measurements, *Spectrochim. Acta Part B* 60 (2005) 968–974.
- [15] H. Lindner, J. Koch, K. Niemax, Production of ultrafine particles by nanosecond laser sampling using orthogonal prepulse laser breakdown, *Anal. Chem.* 77 (2005) 7528–7533.
- [16] J.E. Carranza, D.W. Hahn, Plasma volume considerations for analysis of gaseous and aerosol samples using laser-induced breakdown spectroscopy, *J. Anal. Atmos. Spectrosc.* 17 (2002) 1534–1539.
- [17] D.W. Hahn, M.M. Lunden, Detection and analysis of aerosol particles by laser-induced breakdown spectroscopy, *Aerosol Sci. Technol.* 33 (2000) 30–48.
- [18] D.W. Hahn, J.E. Carranza, G.R. Arsenault, H.A. Johnsen, K.R. Hencken, Aerosol generation system for development and calibration of laser-induced breakdown spectroscopy instrumentation, *Rev. Sci. Instrum.* 72 (2001) 3706–3713.
- [19] V. Hohreiter, D.W. Hahn, Plasma-particle interactions in a laser-induced plasma: implications for laser-induced breakdown spectroscopy, *Anal. Chem.* 78 (2006) 1509–1514.
- [20] V. Hohreiter, J.E. Carranza, D.W. Hahn, Temporal analysis of laser-induced plasma properties as related to laser-induced breakdown spectroscopy, *Spectrochim. Acta, Part B: Atom. Spectrosc.* 59 (2004) 327–333.
- [21] V. Hohreiter, A. Ball, D.W. Hahn, Effects of aerosols and laser cavity seeding on spectral and temporal stability of laser-induced plasmas: applications to LIBS, *J. Anal. At. Spectrom.* 19 (2004) 1289–1294.
- [22] J.E. Carranza, D.W. Hahn, Sampling statistics and considerations for single-shot analysis using laser induced breakdown spectroscopy, *Spectrochim. Acta Part B* 57 (2002) 779–790.
- [23] B.T. Fisher, H.A. Johnsen, S.G. Buckley, D.W. Hahn, Temporal gating for the optimization of laser-induced breakdown spectroscopy detection and analysis of toxic metals, *Appl. Spectrosc.* 55 (2001) 1312–1319.
- [24] J.E. Carranza, K. Iida, D.W. Hahn, Conditional data processing for single-shot spectral analysis by use of laser-induced breakdown spectroscopy, *Appl. Opt.* 42 (2003) 6022–6028.
- [25] D.W. Hahn, W.L. Flower, K.R. Hencken, Discrete particle detection and metal emissions monitoring using laser-induced breakdown spectroscopy, *Appl. Spectrosc.* 51 (1997) 1836–1844.